Ultrafast diffraction conoscopy of the structural phase transition in VO_{2}: Evidence of two lattice distortions

Nardeep Kumar, Armando Rúa, Félix E. Fernández, and Sergiy Lysenko

Ultrafast diffraction conoscopy of VO$_2$ structural phase transition: evidence of two lattice distortions

Nardeep Kumar, Armando Rúa, Félix E. Fernández, and Sergiy Lysenko*
Department of Physics, University of Puerto Rico, Mayaguez, Puerto Rico 00681, USA

Photoinduced phase transitions in complex correlated systems occur very rapidly and involve the interplay between various electronic and lattice degrees of freedom. For these materials to be considered for practical applications, it is important to discover how their phase transitions take place. Here we use a novel ultrafast diffraction conoscopy technique to study the evolution of vanadium dioxide (VO$_2$) from biaxial to uniaxial symmetry. A key finding in this study is an additional relaxation process through which the phase transition takes place. Our results show that the biaxial monoclinic crystal initially, within the first 100–300 fs, transforms to a transient biaxial crystal, and within the next 300-400 fs converts into a uniaxial rutile crystal. The characteristic times for these transitions depend on film morphology and are presumably altered by misfit strain. We take advantage of Landau phenomenology to describe the complex dynamics of VO$_2$ phase transition in the femtosecond regime.

INTRODUCTION

Discovery of a phase transition near room temperature of ~ 340 K, accompanied by a dramatic insulator-to-metal change in electrical properties[1], made VO$_2$ one of the highly investigated strongly correlated electronic materials. VO$_2$ complex phase transition involves electron-electron correlations and electron-lattice interactions[2, 3], which makes it challenging to determine the transition processes[4–6]. Along with temperature[1], VO$_2$ phase transition can also be triggered by a number of different external excitations such as pressure[7], strain[8], doping[9], or light[10]. Out of these external excitations, light with ultra-short laser pulses allows monitoring the phase transition dynamics on ultrafast time scale[11]. In the past recent decades, several enthralling results on VO$_2$, using optical[11–17], terahertz[18–21], X-ray[10, 22–27], and electron diffraction[28–30] methods increased our understanding regarding its phase transition.

VO$_2$ is one of the intensively studied transition metal oxides and a large number of studies have been devoted to the finding of driving mechanisms behind its phase transition. There is a long standing debate over the two mechanisms, Mott or Peierls type, believed to be responsible for the VO$_2$ phase transition[12, 31–35]. Within in this long standing debate, much less attention has been paid to the structural phase transition (SPT) dynamics on femtosecond time scale. An important study related to the VO$_2$ phase transition process involves determining the stages through which a monoclinic biaxial crystal transforms to a rutile uniaxial crystal. One way to study SPT dynamics in femtosecond regime is by tracking only the structural degrees of freedom. Conventional optical pump-probe methods provide a collective response of lattice and electron dynamics. To separate lattice relaxation component from pure electronic response in transient nonlinear optical signal is a nontrivial task and new

experimental approaches are required.

In this paper, we present a novel method of ultrafast diffraction conoscopy (UDC) which allows tracking the transient change of lattice symmetry. By monitoring the transient polarization of scattered light along with the evolution of conoscopy patterns, the UDC reveals two different components of VO$_2$ lattice distortion on subpicosecond time scale. The structural phase transition occurs from monoclinic biaxial to rutile uniaxial crystal and follows a complex phase trajectory via transient intermediate state with biaxial symmetry. Observed nonequilibrium structural dynamics is supported by a quantitative analysis in terms of Ginzburg–Landau formalism.

EXPERIMENT

Sample preparation and characterization

Thin films of VO$_2$ with various thicknesses were grown on single-crystal (110) Al$_2$O$_3$ (A-cut) and (100) Al$_2$O$_3$ (M-cut) substrates by using pulsed laser deposition technique. For these samples, the laser ablation process was performed using an excimer laser (KrF, 248 nm wavelength) with 25 ns pulses. The process was carried out at 4 J/cm^2 fluence with a chamber pressure of 50 mTorr, argon and oxygen gas flows of 10 and 15 standard cubic centimeters per minute, respectively, and substrate temperatures of 550 ^{0}C. The X-ray diffraction (XRD) patterns of all VO$_2$ films evidenced single monoclinic M$_1$ phase at room temperature, with good off-plane and in-plane orientation with respect to the sapphire substrates which can be described as epitaxial. Atomic Force Microscopy (AFM) and XRD analyses were performed to verify the quality and orientation of the films, as shown in Supplementary Figs. 2 and 3 respectively[36].
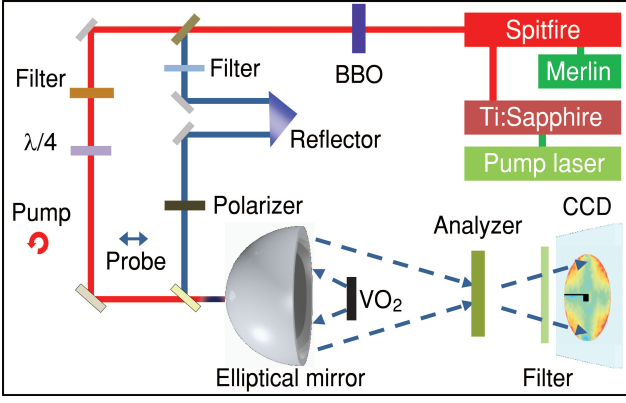
FIG. 1. Schematics of the experimental setup for polarization resolved light scattering measurements.

Ultrafast diffraction conoscopy

The experiment to study light-induced SPT dynamics of VO_2 was performed with a scatterometer setup schematically shown in Fig. 1. A titanium sapphire laser (Ti:Sapphire) provides ultrashort pulses with a central wavelength of $\lambda = 800$ nm and a repetition rate of 80 MHz. The output from Ti:Sapphire is sent to a regenerative amplifier (Spectra-Physics:Spitfire) which is pumped by a Nd:YLF laser (Merlin) of 8 W average output and a repetition rate of 1 KHz. The regenerative optical amplifier provides 800 nm wavelength output with pulse time duration between 80 and 130 fs and 1 KHz repetition rate, which is used as a pump beam. The second harmonic pulse, which acts as a probe, with a central wavelength of 400 nm, is obtained by using a Beta Barium Borate (BBO) nonlinear crystal.

The phase transition was triggered by the circularly polarized pump pulse focused to a spot size of 0.6 mm. Circular polarization was used to avoid possible artifacts owing to the photoinduced anisotropy of VO_2 electronic density that is not actually related to lattice symmetry. To monitor the phase transition, the vertically polarized probe pulse was focused into a tighter spot of 70 μm diameter. Both pump and probe pulses were incident normal to the sample surface, which was mounted on a rotational holder. The time delay between pump and probe pulses was controlled by using a retro-reflector in the probe arm. Scattered light from the sample was collected by an elliptical mirror which focused the light to a charge-coupled device (CCD). The pump beam was prevented from reaching the detector by using a color filter.

The scattering distribution signal was measured and mapped as a Bidirectional-Scatter-Distribution-Function (BSDF) versus polar angle θ and azimuthal angle φ. The BSDF is defined as follows[48]:

$$BSDF(\theta, \varphi) = \frac{1}{I_0} \left(\frac{dI_{scatt}(\theta, \varphi)}{d\Omega} \right) \frac{1}{cos\theta} \qquad (1)$$

where I_0 is the intensity of incident light, and dI_{scatt} is the intensity of light scattered into solid angle $d\Omega$. To record the conoscopy images an analyzer is inserted between CCD and elliptical mirror at horizontal polarization. The transient scattering signal is maximal when the VO_2 optical axis is tilted to a specific angle with respect to the probe polarization so that there is a stronger change of elliptical polarization of scattered light during the SPT. Therefore, samples were rotated to a position of highest transient modulation of scattering signal. The measurements were performed at room temperature.

The conoscopy technique is based on angle-resolved elastic light scattering and employs two crossed linear polarizers before and after the elliptical mirror (Fig. 1). Light scattering is a process directly related to surface irregularities and optical properties and provides information about material inhomogeneities[49–52]. UDC technique is useful for statistical analysis of transient crystallographic symmetry of polydomain highly orientated films with a thickness about one order of magnitude less than the laser probe wavelength. This method is based on the fact that the crystal anisotropy produces optical birefringence and splits linearly polarized light into two mutually orthogonal components with different phase velocities. Due to cumulative phase difference of these components, the scattered light becomes elliptically polarized. The degree of elliptical polarization and the shape of conoscopy pattern were monitored by using a CCD detector equipped by a linear polarizer (analyzer).

UDC allows separating signals related only to the lattice symmetry transformation from other types of signals (band filling, change of optical constants during phase transition, etc.), which is an important advantage of this technique. A noticeable contribution in light depolarization arises from Rayleigh scattering which allows monitoring birefringence of microcrystals with sizes much less than the light wavelength.

RESULTS

Figure 2(a) shows the Bidirectional-Scatter-Distribution-Function (BSDF) indicatrices of hemispherical light scattering from a 40 nm thick VO_2 film on a sapphire substrate (A-cut) as a function of both polar and azimuthal angles. The distinctive conoscopy patterns at different probe delays are outlined by dashed isophotes. For these scans, the energy fluence of the pump pulses was 14 mJ/cm². In the first few hundred femtoseconds, the scattering signal consists of two hyperbolas, similar to biaxial isogyres (see Fig. 3(d) in the Supplemental Material [36]), in opposite quadrants, which transform to a cross-like pattern, similar to uniaxial isogyres (see Fig. 3(b) in the Supplemental Material [36]), at the end of the phase transition. Figure 2(c) represents the cross-sections of the scattering
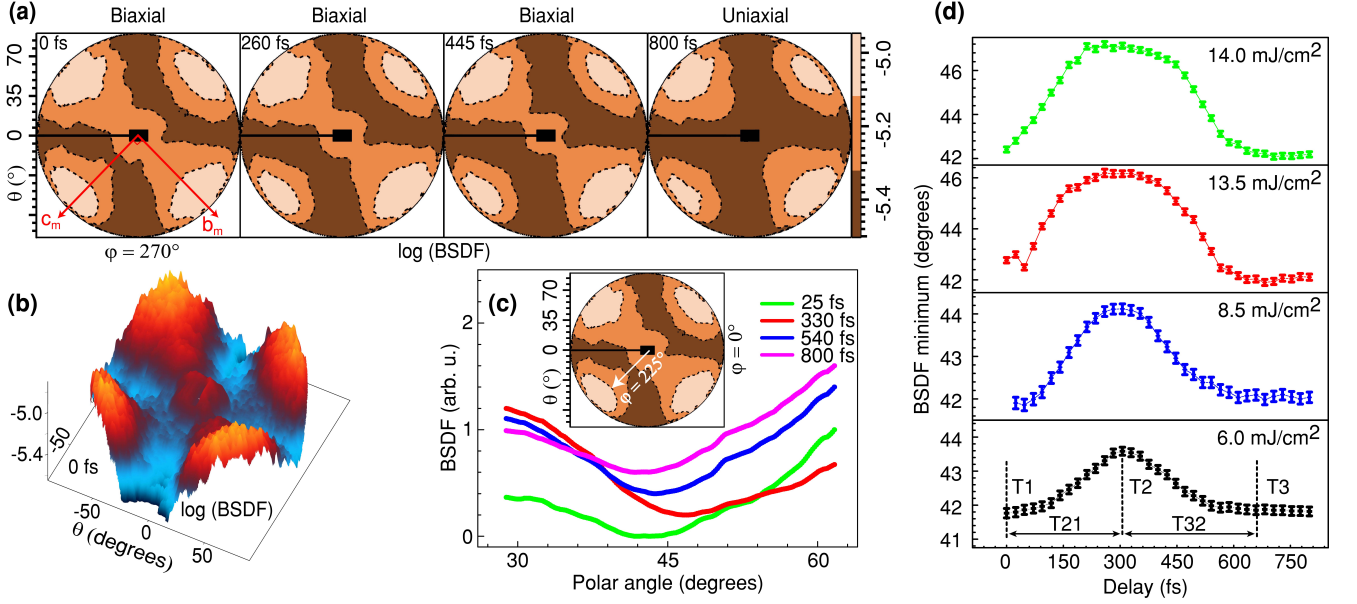
FIG. 2. Ultrafast diffraction conoscopy of VO_2 film on A-cut Al_2O_3. (a) Evolution of the light scattering indicatrix showing the transformation of biaxial isogyres to uniaxial isogyres. The distinctive conoscopy patterns are outlined by dashed isophotes. The black rectangular region along with a black bar shows the location of the sample holder. (b) Three-dimensional view of light scattering indicatrix showing conoscopy patterns at 0 fs. (c) Cross-sections of the scattering indicatrix along an azimuthal angle $\varphi=225^0$ for 25 fs, 330 fs, 540 fs and 800 fs. The arrow inside the inset shows the azimuthal direction of the cross-sections. (d) Temporal position of BSDF minimum of scattering indicatrix cross-section at $\varphi=225^0$ for various pump fluences. Error bars represent the standard deviation obtained from multiple measurements to collect BSDF minimum shift.

indicatrix for probe delays of 25 fs, 330 fs, 540 fs, and 800 fs, along an azimuthal angle $\varphi=225^0$. The most obvious non-trivial observation from these BSDF curves is that the intensity minimum shifts significantly during the SPT interval. This noticeable shift reflects the change in the conoscopy pattern as a result of lattice transformation.

To investigate the evolution of the VO_2 system through SPT, we take polar angles corresponding to BSDF minimum of scattering indicatrix curves at various probe delays and plot, as shown in Fig. 2(d), for different pump fluences. From this BSDF minimum shift trend, two distinct processes can be resolved: (1) during the first $\sim$300 fs the initial monoclinic lattice of VO_2 transforms into a nonequilibrium biaxial phase which appears as an increase of the angular position of the BSDF minimum and (2) after $\sim$300 fs the angular position of the BSDF minimum starts to decrease, attaining a constant value within 500-700 fs. In discussing this transition, we define some characteristic times in Fig. 2(d), where T1 time represents zero delay, T2 time is defined by the extreme of minimum change and T3 is where the shift reaches a steady level. Tji is defined as the time difference between the ith and j^{th} times. The shift reaches a peak at T2 within 300 fs after zero delay. After a period of ΔT21 = 300 fs, the shift starts to decrease for a period of ΔT32 = 300-400 fs and reaches a minimum at T3. After that, the shift reaches a steady level, which corresponds to the

end of the subpicosecond phase transition.

The light scattering intensity is proportional to the squared value of optical polarizability and surface roughness[48, 53]. The absolute value of the VO_2 dielectric constant and, as a consequence, its polarizability is lower for the metallic phase[54]. As shown in Refs. 55 and 56, the surface geometry does not change during ultrafast phase transition, and the light scattering intensity decreases due to transient change of VO_2 optical properties. Hence, if the phase transition is a single stage process, then the BSDF minimum should shift monotonically. However, the fact that it first increases and then decreases indicates that the initial monoclinic lattice transforms to a different biaxial crystal. Although the actual crystal symmetry of this transient phase is unknown, it is definitely a biaxial crystal, as evidenced in the indicatrix sequence in Fig. 2(a). Furthermore, the increase of pump fluence results in a larger transient change of this angular position due to a higher level of photoinduced metastability accompanied by stronger lattice distortion.

In order to further investigate the rich dynamics of the VO_2 phase transition and also to support results of Fig. 2(d), we map the UDC data as a relative change of measured signal ΔBSDF(t)/BSDF(0), where ΔBSDF(t) = BSDF(t)-BSDF(0) as shown in Fig. 3(a). These data represent the evolution of polarization state of light scattering from VO_2 film. Here an emerging rectangular region with larger positive ΔBSDF(t)/BSDF(0) values,
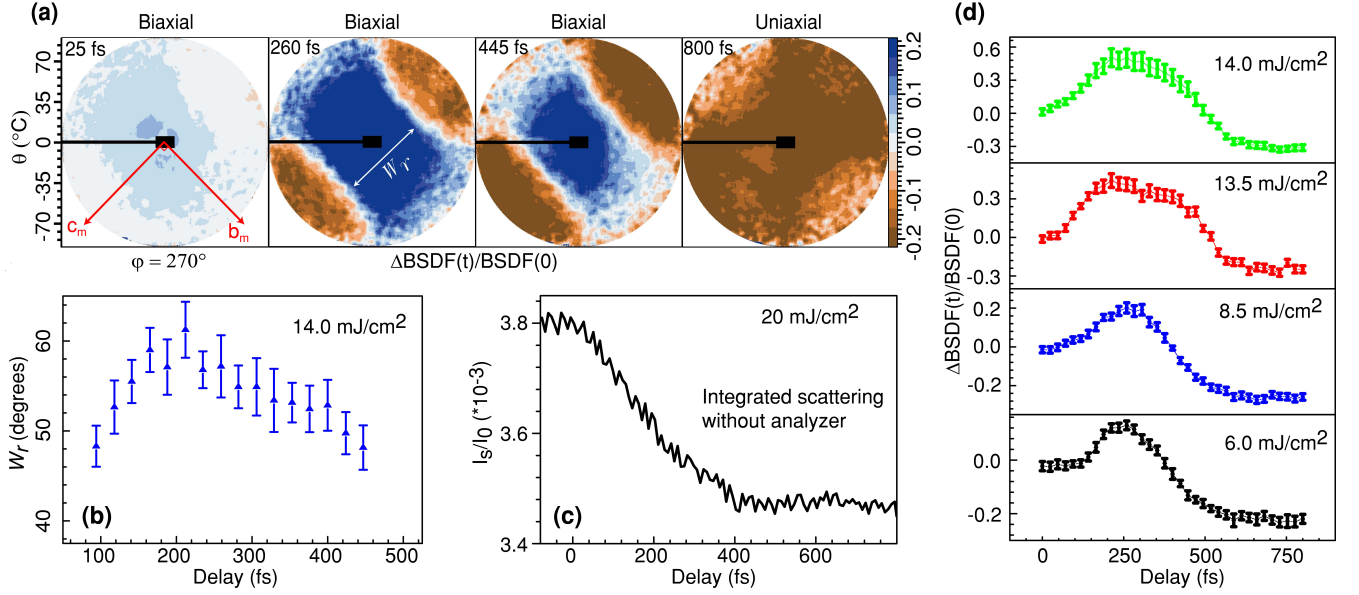
FIG. 3. Evolution of polarization state of light scattering from VO_2 film on A-cut Al_2O_3. (a) Relative change of UDC indicatrix $\Delta BSDF(t)/BSDF(0)$; A rectangular region, ascribed to a multistage phase transition, emerging in the beginning of the phase transition reaches to a peak between 250-350 fs and then starts to decrease and disappears after 500-700 fs (see Movie 1 in the Supplemental Material [57]). (b) Change of the width (Wr) of the dark rectangular region at an azimuthal angle of $\varphi=225^0$ with respect to the probe delay. Width was measured from 95 fs to 470 fs due to the low resolution outside this interval. (c) Light scattering, integrated over the hemisphere without analyzer, as a function of probe delay for a pump fluence of 20 mJ/cm^2. (d) UDC: cross-section of $\Delta BSDF(t)/BSDF(0)$ at $\varphi=225^0$ for various pump fluences. Error bars represent the standard deviation obtained from multiple measurements.

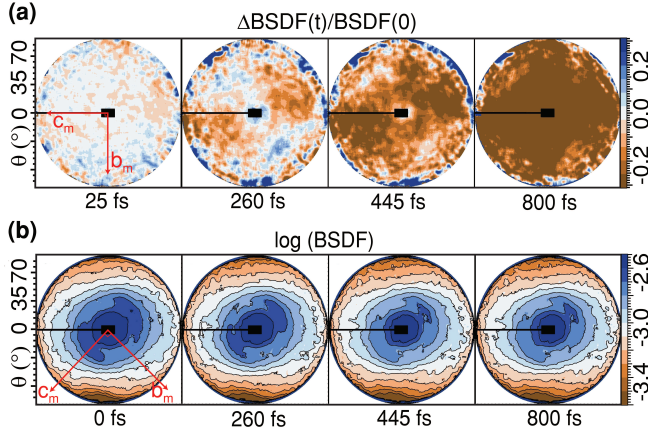FIG. 4. Transient light scattering from VO_2 films on A-cut Al_2O_3. (a) Relative change $\Delta BSDF(t)/BSDF(0)$ of UDC indicatrix. The sample is rotated by -45^0 from the original orientation in Figs. 2 and 3. (b) Evolution of light scattering indicatrix without an analyzer.

peaks at 250-350 fs and then starts to decrease and disappears after 500-700 fs (see Movie 1 in the Supplemental Material [57]). This behavior can be ascribed to a two-stage phase transition which causes an increase followed by a decrease of differential scattering. It is noted that the time for the maximum differential scattering signal

coincides with the characteristic time T2 for BSDF minimum [see Fig. 2(d)].

To trace the change of light polarization due to lattice transformation into an intermediate transient state, we define an arbitrary parameter Wr as the width of the rectangular region at an azimuthal angle of $\varphi=225^0$. The measured width (Wr) in angular units for various time delays is shown in Fig. 3(b). Due to the low resolution near zero delay, we measured Wr starting from 100 fs. Change of the width with time delay follows the same trend as seen from the position of BSDF minimum in Fig. 2(d). From these results, we conclude that the observed phase transition is dominated by biaxial symmetry, which changes to uniaxial within 500-700 fs time interval. Our results for the shift of BSDF minimum and relative change of differential scattering provide solid evidence for the existence of a two-stage phase transition in VO_2. Next, we explore the phase transition trend using total integrated scattering over hemisphere without analyzer and compare the results with those for UDC patterns. Figure 3(c) shows the total integrated scattering signal I_S/I_0 as a function of the probe delay for the first 800 fs. From this curve, we deduced the phase transition characteristic time on the order of 400 fs.

The complex dynamics of photoinduced phase transition results in a gradual change of the VO_2 band structure on femtosecond time scale. Ordinary pump-probe
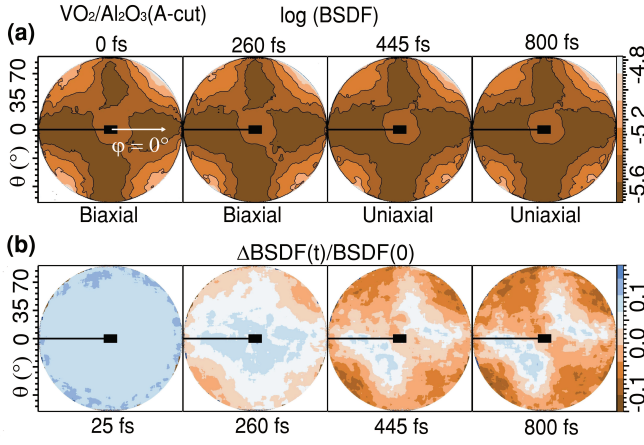
FIG. 5. The light scattering from 80 nm thick VO_2 film on A-cut Al_2O_3. (a) Evolution of UDC indicatrix during the transformation of VO_2 from biaxial to the uniaxial crystal at 14.0 mJ/cm^2 excitation. (b) Relative change of transient conoscopy signal $\Delta BSDF(t)/BSDF(0)$.

FIG. 6. The light scattering from 80 nm thick VO_2 films on M-cut Al_2O_3. (a) Evolution of UDC indicatrix during transformation of VO_2 from biaxial to the uniaxial crystal at 14.0 mJ/cm^2 laser excitation. (b) Transient change of relative conoscopy signal $\Delta BSDF(t)/BSDF(0)$.

optical techniques which utilize transient transmission, reflection or total integrated scatter show a monotonic step-like change of the optical signal as VO_2 switches to its final rutile phase. However, these techniques only partially resolve lattice relaxation dynamics, and many features remain hidden. After rigorous analysis of experimental data, several works[16, 28, 29, 56, 58] reported the presence of at least two stages of phase transition. Here, applying UDC technique the two stages of SPT process can be clearly resolved on a femtosecond time scale as shown in Fig. 3(d). As it was expected, when VO_2 completely switched into a final rutile phase within 700 fs, the total change of the scattering signal is nearly independent on pump fluence. However at ~ 300 fs, increasing excitation level results in the significant rise of $\Delta BSDF(t)/BSDF(0)$ UDC signal. This behavior is associated with higher level of photoinduced metastability which provides stronger transient lattice distortion and, as a consequence, higher depolarization of scattered light.

In order to demonstrate the influence of crystal orientation on transient UDC indicatrix, we rotated the sample by -45^0, from the original orientation in Figs. 2 and 3. The resulting differential UDC patterns are shown in Fig. 4(a). At this orientation of the sample, the b_m axis of VO_2 lattice coincides with the polarization plane of the probe beam. As a result, the $\Delta BSDF(t)/BSDF(0)$ signal drops monotonically, without showing noticeable light depolarization.

To compare UDC results with ultrafast light scattering, we collected scattering data by removing the analyzer from the setup. The BSDF indicatrices, measured as a function of both θ and φ, with respect to probe delay, are shown in Fig. 4(b). As expected, the scattering indicatrices show only a continuous decrease of the signal without any noticeable intermediate transition, same
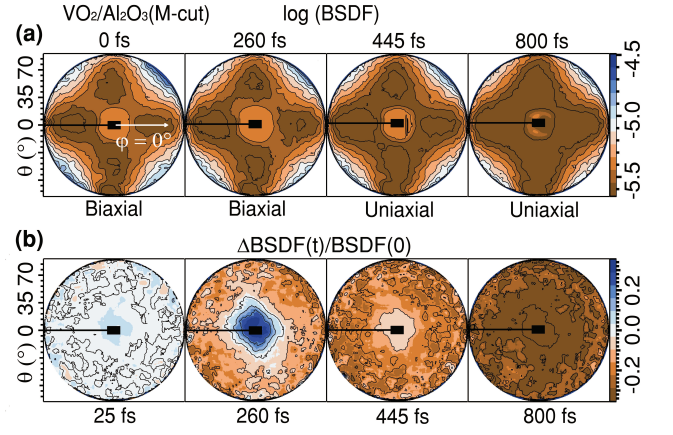
as seen for total integrated scattering [Fig. 3(c)]. An elliptical type pattern can be observed in these indicatrices due to the multidomain epitaxial nature of the film, which means that there are strongly preferential lateral orientations of the VO_2 lattice with respect to the substrate. These results highlight the relevance of the UDC for studies of the transformation.

To explore the effects of thickness and misfit strain, we also investigated thicker VO_2 (80 nm) samples grown on A-cut (110 plane) and M-cut (100 plane) sapphire substrates. The azimuthal orientation of the samples was set to obtain maximal differential, $\Delta BSDF(t)/BSDF(0)$, signal. Time-resolved diffraction conoscopy indicatrices from VO_2 films on A-cut and M-cut substrates are shown in Figs. 5 and 6 respectively. The scattering data for all the samples are compared with respect to their orientation along the probe direction. By comparing 40 nm and 80 nm VO_2 samples on A-cut substrates the conoscopy patterns in the case of the thicker film are less sharp. However, the change from biaxial to uniaxial symmetry is still visible [Fig. 5]. Similarly, for the 80 nm thick VO_2 film on M-cut sapphire the change in conoscopy patterns clearly indicates biaxial to uniaxial transformation. Differential scattering [Fig. 6(b)] shows a sharp square-like feature due to the preferable orientation of VO_2 grains and domains on single-crystal Al_2O_3 substrate, as confirmed by x-ray measurements versus azimuthal orientation of the sample (see Figs. 2(c) and 2(d) in the Supplemental Material [36]).

Figure 7 shows the cross-sections of UDC patterns along azimuthal directions with stronger light depolarization, for all the three samples. As can be clearly seen in the case of the 40 nm thick VO_2 film on A-cut sapphire, the first stage in the transition process reaches an extreme, shown by a vertical dashed line, in about 250–
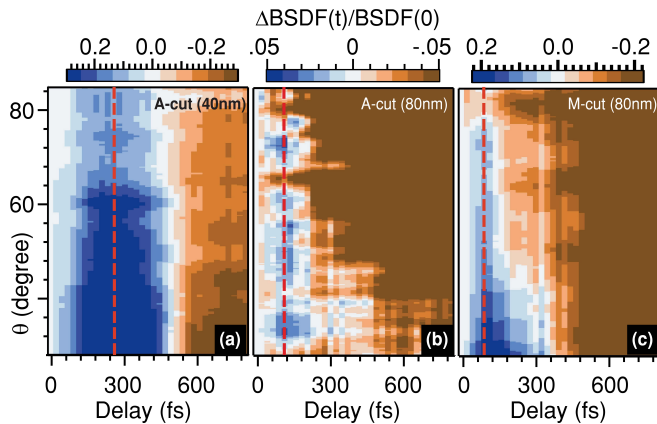
FIG. 7. Cross-sections of UDC patterns from three VO$_2$ samples for different polar angles at azimuthal angle $\varphi=285^0$ with respect to time delay. ΔBSDF(t)/BSDF(0) distribution for (a) 40 nm VO$_2$ film on A-cut Al$_2$O$_3$, (b) 80 nm VO$_2$ films on A-cut Al$_2$O$_3$, (c) 80 nm VO$_2$ films on M-cut Al$_2$O$_3$. Cross-section maps clearly show the difference between phase transition dynamics in three VO$_2$ samples. In the case of 40 nm sample on A-cut sapphire, the first stage in the transition process reaches an extreme in about 300 fs and is then followed by a second stage which decays within 300–400 fs. The first stage is twice faster in thicker samples on A- and M-cut sapphire substrates. Vertical dashed lines indicate the maximum of ΔBSDF(t)/BSDF(0) signal related to the intermediate biaxial state.

300 fs and is then followed by a second stage which decays within next 300–400 fs. However, in the case of thicker samples on A- and M-cut sapphire substrates the first stage occurs twice faster than for the thin sample. This implies that the intermediate biaxial state lasts longer in thinner films, which are expected to have higher strain, as compared to thicker films.

DISCUSSION

Time-resolved diffraction conoscopy allows monitoring the transformation of lattice symmetry in epitaxial or textured films with thicknesses much smaller than the wavelength of incident light. Moreover, obtained data are statistically averaged over thousands of microcrystals within the illuminated area. Thus, UDC technique can provide information about structural relaxation for thin polydomain films, as long as transient light depolarization or a transient conoscopy patterns can be detected. The presence of VO$_2$ domains with different orientations results in a smearing of the conoscopy patterns; however, this does not affect the pathway of structural transformation. We note that for all the studied films we observed very similar transient behavior and a pronounced change of scattering signal and conoscopy patterns.

The biaxial to uniaxial ultrafast phase transition in VO$_2$ takes place in two stages, and can be considered as related to two different lattice distortions similar to those discussed by Goodenough[2]. It should be noted here that we have observed two components of the SPT for three VO$_2$ films with substantially different morphology, and these two components are associated with two different characteristic lattice distortions with different relaxation times. Moreover, for the thinner film, which is expected to have a higher misfit strain, the characteristic relaxation time of the first transition stage is 250-300 fs [Figs. 2, 3 and 7(a)] which is twice slower than for the thicker films [Figs. 7(b) and 7(c)]. This fact suggests that the strain is one of the key parameters controlling ultrafast lattice relaxation dynamics.

While two distinct lattice relaxation processes are observed, the starting point of the second process is difficult to resolve with high accuracy. It is very likely that the light pulse triggers two lattice relaxation processes simultaneously, but the internal strain in the film alters the relaxation time of each characteristic lattice distortion and affects the total pathway of the SPT which appears as a two-stage process. The first stage of SPT is related to the initial transition to a transient state with biaxial symmetry. This process is mainly associated with the antiferroelectric lattice distortion. The second stage of SPT is related to the lattice transformation into the rutile phase, with uniaxial symmetry, and can be assigned to V-V bonding.

Here we note that the total light-induced SPT in a thin VO$_2$ film occurs simultaneously in all grains of the film within several hundred femtoseconds. Several studies of transient surface statistics[55, 56] have shown the absence of coexistence of different VO$_2$ phases during the ultrafast phase transition. While slight variation of characteristic transition time was observed versus grain size, the pathway of SPT was identified as a coherent process across all spatial frequencies of the surface. Moreover, on femto- and picosecond time scales only short-range phonon interactions take place[55, 56]. As a result, the ultrafast phase transition does not noticeably contribute to formation of new domains within several picoseconds.

The ultrafast first-order phase transition can be analyzed in terms of Ginzburg-Landau theory[59–61]. The experimentally observed SPT dynamics can be supported by modelling of thermodynamic potential Φ for photoexcited VO$_2$ as shown in Fig. 8. To estimate the profile of thermodynamic potential, we performed calculations of molecular dynamics and measured transient reflection and transmission of VO$_2$ films (see Supplemental Material [36]). Measurements of relaxation rates on picosecond time scale allowed us to estimate the profile of Φ. Two different components of VO$_2$ lattice distortion revealed by UDC can be associated with two effective ion displacements x_1 and x_2, which correspond to antiferroelectric distortion and V-V bonding respectively. Taking into account only insulating M$_1$ and metallic R-phase of VO$_2$, the thermodynamic potential Φ consists of two po-

tential wells separated by a barrier ΔG. The two-well potential model does not imply the presence of an intermediate state of VO_2 explicitly, but it can be used for analyses of two different lattice distortions.

The two-well lattice thermodynamic potential Φ can be described by employing the following ansatz[61]:

$$\Phi = \frac{\alpha(F)}{2}(x_1^2 + x_2^2) + \frac{\beta_1}{4}(2x_1x_2)^2 + \frac{\beta_2}{4}(x_1^2 - x_2^2)^2 \\ + \frac{\gamma}{6}(x_1^2 + x_2^2)^3 \qquad (2)$$

where F is laser fluence and $\alpha(F)$, β_1, β_1 and γ are experimentally derived constants. These constants were estimated from additional measurements of the slower (picosecond) component of VO_2 relaxation dynamics which was detected after the ultrafast subpicosecond transition at excitation fluence below 30 mJ/cm^2.

We assume that the concentration of photoexcited free carriers is the main factor that alters Φ, and x_1 and x_2 correspond to the whole displacement of VO_2 sublattices during antiferroelectric distortion and V-V bonding, correspondingly. The VO_2 lattice motion is oscillatory in nature and it has been shown by many groups that it oscillate with frequency of 6 THz[3, 16–18, 62, 63]. Taking into account the relaxation nature of these oscillations, we obtain the equation of motion[64]:

$$\ddot{x}_i + 2g_i\dot{x}_i = -\frac{1}{\widetilde{m}}\frac{\partial\Phi}{\partial x_i} \qquad (3)$$

where $\widetilde{m}$ is the effective mass and g_i is the damping coefficient, related to the experimentally measured transition rate for each distortion i of the phase transition. For two observed distortions, damping coefficients $g_1 = 6.7\times10^{12}$ s^{-1} and $g_2 = 2.1\times10^{12}$ s^{-1} were calculated using experimental data of figures 2 and 3. Using the thermodynamic potential Φ and frequency 6 THz of optical phonon mode, the effective mass $\widetilde{m}$ was estimated as 1.7×10^{-25} kg.

Figure 8(a) shows the pathway of the energy relaxation obtained by numerical integration of equation (3) for the ultrafast first-order phase transition. Here, the photoexcitation of the free carriers instantaneously modifies the thermodynamic potential Φ by screening the Coulomb repulsion and switching the VO_2 lattice into a nonequilibrium excited state [65, 66]. In case of absence of internal strain, our model assumes that the relaxation rates for two distortions x_1 and x_2 are equal. As a result, the phase trajectory of the phase transition is just a simple transition from monoclinic phase to rutile phase denoted by a straight dashed line "M$_1$-R" on the potential landscape in Fig. 8(a). This transition would result in monotonic decrease of light depolarization during the transition. However, experimental observations of lattice dynamics by UDC shows significant transient depolarization of light scattering for all samples due to deviation of actual phase trajectory from "M$_1$-R" straight line. Since
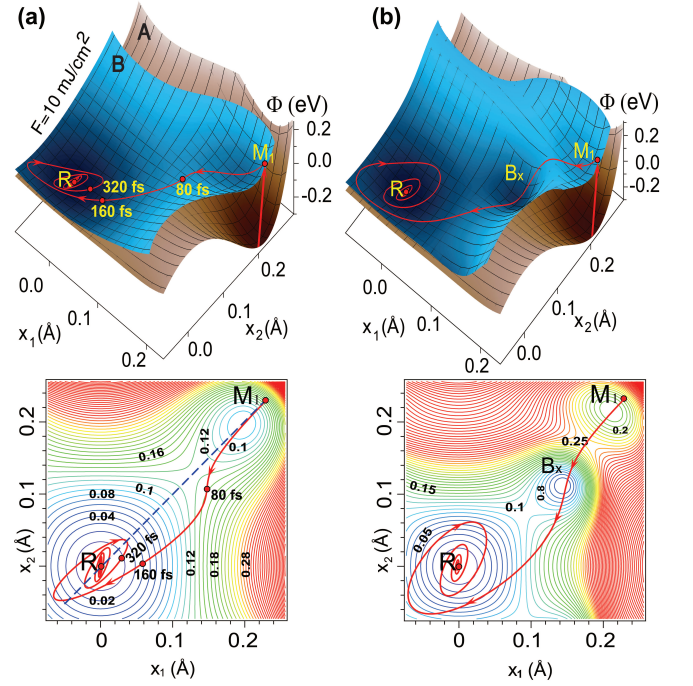

FIG. 8. Phase trajectory of photoexcited VO_2. The solid line with arrows shows the pathway of the energy relaxation after photoinduced change of thermodynamic potential. Two potential energy surfaces, marked by A and B, correspond to unperturbed and photoexcited states of VO_2 respectively. (a) A double-well potential case. This model implies the presence of only M$_1$ and R phases. Dashed line indicates the phase trajectory for the case of equal relaxation rates for antiferroelectric distortion (x_1) and V-V bonding (x_2). (b) A triple-well thermodynamic potential. The possible intermediate phase is denoted by B$_x$.

the lifetime of transient biaxial phase depends on type and thickness of epitaxial film [Fig. 7], it is believed that the internal misfit strain increases this deviation via difference in the relaxation rate for antiferroelectric distortion and V-V bonding.

The UDC data for 40 nm VO_2/Al_2O_3(A-cut) shows significant rise of transient depolarization within 300 fs [Figs. 2 and 7(a)], a timescale which is nearly twice longer than the oscillation period of VO_2 optical phonons (see Section 5 in the Supplemental Material [36]). This relatively long time can correspond not only to different relaxation rates for distortions x_1 and x_2, but also to the presence of an intermediate biaxial phase and additional third potential well on the Φ landscape denoted by B$_x$, as shown in Fig. 8(b). Upon light-induced phase transition the lattice symmetry changes from monoclinic to rutile via B$_x$, moving along some complex phase trajectory.

Recently, several studies using tempearature[17, 67–70], pressure[71–74], light[29, 35, 58, 66] and voltage[27] demonstrate that VO_2 phase transition takes place through an intermediate phase with monoclinic symmtery. Bai et al. suggest the presence of several new

phases (e.g. distorted M_1, orthorhomic, X phase) under high pressure[72]. In the case of photoinduced SPT, the initial excited state corresponds to M_1 phase, while the transient biaxial phase B_x can be M_2 or orthorhombic phase. However, the exact symmetry of B_x phase cannot be determined by optical UDC technique. Nevertheless, transient B_x phase is definitely a biaxial phase which is different from initial M_1 and final rutile phase.

The presence of two different lattice distortions in ultrafast phase transition reveals a resemblance between light-induced and thermally induced crystallographic transtions in terms of Goodenough's model, proposed in his seminal work[2]. According to Goodenough, two distinguishable components of lattice distortion are present: antiferroelectric distortion into an orthorhombic structure and homopolar V-V bonding along the a_m axis. For pure and unstrained VO_2 these distortions occur at the same temperature. However, doping or mechanical strain both separate the temperatures at which they occur. In our case, it is very likely that the strain affects the SPT in a similar way, resulting in structural transition from monoclinic to an intermediate phase before transforming to a rutile symmetry. This concept agrees with Goodenough's prediction about an orthorhombic intermediate phase which is also biaxial in nature. There have been numerous studies demonstrating that the strain is one of the key parameters which alters the phase transition pathway [23, 69, 75–84]. Laverock *et al.* provide conclusive evidence that the observed intermediate phase is accessible in the ground state at ambient temperatures and pressures in epitaxially strained VO_2[69].

For a triple-well thermodynamic potential the quantitative theoretical analysis of the SPT dynamics becomes rather difficult. However, qualitative estimation shows that the additional potential well can noticeably increase the transient time of the nonequilibrium biaxial state. The presence of an additional potential well in Φ can significantly increase the difference in the relaxation rate for antiferroelectric distortion and V-V bonding and, as a result, increase the depolarization time of scattered light observed by UDC. During this SPT, the relaxation rate can be a function of time (i.e. damping of vibrational modes can change during SPT). Taking into account significant differences in relaxation dynamics of epitaxial VO_2 films on different substrates [Fig. 7], it is very likely that the depth of the potential well B_x for transient intermediate phase depends on film morphology and internal strain.

CONCLUSION

In conclusion, we have shown that the femtosecond pump-probe diffraction conoscopy is a powerful technique to track the structural phase transition dynamics in complex correlated materials. A pronounced two-stage pro-

cess in the phase transition of VO_2 was observed with two distinct characteristic times. After the phase transition is triggered by a light pulse, the monoclinic biaxial crystal transforms to a transient biaxial crystal which is the first stage of the phase transition, lasting for 100–300 fs. The second stage lasts next 300–400 fs and is related to the lattice transformation from transient biaxial phase into the rutile uniaxial phase. It is most likely that the internal misfit strain in epitaxial film alters the observed characteristic relaxation times. By applying Ginzburg–Landau formalism it is shown that the observed two-stage UDC dynamics is originated from two lattice distortions with different relaxation times. According to Goodenough's model of VO_2 lattice instability these distortions can be associated with antiferroelectric lattice distortion and homopolar V-V bonding.

----

* sergiy.lysenko@upr.edu

[1] F. J. Morin, Phys. Rev. Lett. **3**, 34 (1959).
[2] J. B. Goodenough, J. Solid State Chem. **3**, 490 (1971).
[3] A. Cavalleri, T. Dekorsy, H. H. Chong, J.-C. Kieffer, and R. W. Schoenlein, Phys. Rev. B **70**, 161102 (2004).
[4] M. Imada, A. Fujimori, and Y. Tokura, Rev. Mod. Phys. **70**, 1039 (1998).
[5] E. Dagotto, Science **309**, 257 (2005).
[6] P. A. Lee, N. Nagaosa, and X.-G. Wen, Rev. Mod. Phys. **78** (2006).
[7] J. Sakai and M. Kurisu, Phys. Rev. B **78**, 033106 (2008).
[8] T. Kikuzuki and M. Lippmaa, Appl. Phys. Lett. **70**, 132107 (2004).
[9] X. Tan, T. Yao, R. Long, Z. Sun, Y. Feng, H. Cheng, X. Yuan, W. Zhang, Q. Liu, C. Wu, Y. Xie, and S. Weib, Sci. Rep. **2**, 466 (2012).
[10] A. Cavalleri, C. Tóth, C. W. Siders, J. A. Squier, F. Ráksi, P. Forget, and J. C. Kieffer, Phys. Rev. Lett. **87**, 237401 (2001).
[11] M. F. Becker, A. B. Buckman, R. M. Walser, T. Lepine, P. Georges, and A. Brun, Appl. Phys. Lett. **65**, 1507 (1994).
[12] M. M. Qazilbash, M. Brehm, B. Chae, P.-C. Ho, G. O. Andreev, B. Kim, S. Yun, A. V. Balatsky, M. B. Maple, F. Keilmann, H. Kim, and D. N. Basov, Science **318**, 1750 (2007).
[13] S. Lysenko, A. Rua, V. Vikhnin, J. Jimenez, F. Fernandez, and H. Liu, Appl. Surf. Sci. **252**, 5512 (2006).
[14] K. Appavoo, B. Wang, N. F. Brady, M. Seo, J. Nag, R. P. Prasankumar, D. J. Hilton, S. T. Pantelides, and R. F. Haglund, Nano Lett. **14**, 1127 (2014).
[15] A. C. Jones, S. Berweger, J. Wei, D. Cobden, and M. B. Raschke, Nano Lett. **10**, 1574 (2010).
[16] S. Wall, L. Foglia, D. Wegkamp, K. Appavoo, J. Nag, R. F. Haglund, J. Stähler, and M. Wolf, Phys. Rev. B **87**, 115126 (2013).
[17] H.-T. Kim, Y. W. Lee, B.-J. Kim, B.-G. Chae, S. J. Yun, K.-Y. Kang, K.-J. Han, K.-J. Yee, and Y.-S. Lim, Phys. Rev. Lett. **97**, 266401 (2006).
[18] C. Kübler, H. Ehrke, R. Huber, R. Lopez, A. Halabica, R. F. Haglund, and A. Leitenstorfer, Phys. Rev. Lett.

99, 116401 (2007).

[19] D. J. Hilton, R. P. Prasankumar, S. Fourmaux, A. Cavalleri, D. Brassard, M. A. El Khakani, J. C. Kieffer, A. J. Taylor, and R. D. Averitt, Phys. Rev. Lett. **99**, 226401 (2007).

[20] X. Xue, M. Jiang, G. Li, X. Lin, G. Ma, and P. Jin, J. Appl. Phys. **114** (2013).

[21] M. Nakajima, N. Takubo, Z. Hiroi, Y. Ueda, and T. Suemoto, Appl. Phys. Lett. **92**, 011907 (2008).

[22] D. B. McWhan, M. Marezio, J. P. Remeika, and P. D. Dernier, Phys. Rev. B **10**, 490 (1974).

[23] M. Hada, K. Okimura, and J. Matsuo, Phys. Rev. B **82**, 153401 (2010).

[24] M. W. Haverkort, Z. Hu, A. Tanaka, W. Reichelt, S. V. Streltsov, M. A. Korotin, V. I. Anisimov, H. H. Hsieh, H. J. Lin, C. T. Chen, D. I. Khomskii, and L. H. Tjeng, Phys. Rev. Lett. **95**, 196404 (2005).

[25] A. Cavalleri, M. Rini, H. H. W. Chong, S. Fourmaux, T. E. Glover, P. A. Heimann, J. C. Kieffer, and R. W. Schoenlein, Phys. Rev. Lett. **95**, 067405 (2005).

[26] A. Cavalleri, H. H. Chong, S. Fourmaux, T. E. Glover, P. A. Heimann, J. C. Kieffer, B. S. Mun, H. A. Padmore, and R. W. Schoenlein, Phys. Rev. B **69**, 153106 (2004).

[27] B.-J. Kim, Y. W. Lee, S. Choi, J.-W. Lim, S. J. Yun, H.-T. Kim, T.-J. Shin, and H.-S. Yun, Phys. Rev. B **77**, 235401 (2008).

[28] P. Baum, D.-S. Yang, and A. H. Zewail, Science **318**, 788 (2007).

[29] V. R. Morrison, R. P. Chatelain, K. L. Tiwari, A. Hendaoui, A. Bruhács, M. Chaker, and B. J. Siwick, Science **346**, 445 (2014).

[30] V. A. Lobastov, J. Weissenrieder, J. Tang, and A. H. Zewail, Nano Lett. **7**, 2552 (2007).

[31] H. T. Kim, B. G. Chae, D. H. Youn, S. L. Maeng, G. Kim, K. Y. Kang, and Y. S. Lim, N. J. Phys. **6**, 52 (2004).

[32] J. M. Booth and P. S. Casey, Phys. Rev. Lett. **103**, 86402 (2009).

[33] S. Kim, K. Kim, C.-J. Kang, and B. Min, Phys. Rev. B **87**, 195106 (2013).

[34] T. Yao, X. Zhang, Z. Sun, S. Liu, Y. Huang, Y. Xie, C. Wu, X. Yuan, W. Zhang, Z. Wu, *et al.*, Phys. Rev. Lett. **105**, 226405 (2010).

[35] T. L. Cocker, L. V. Titova, S. Fourmaux, G. Holloway, H. C. Bandulet, D. Brassard, J. C. Kieffer, M. A. El Khakani, and F. A. Hegmann, Phys. Rev. B **85**, 155120 (2012).

[36] See Supplemental Material at [url] for additional figures and accompanying text, which includes Refs. [37–47].

[37] Z. P. Wu, A. Miyashita, I. Nashiyama, and H. Naramoto, Philos. Mag. Lett. **79**, 813 (1999).

[38] K. Hefferan and J. O'Brien, *Earth materials*, (Wiley-Blackwell, 2010).

[39] B. T. O'Callahan, A. C. Jones, J. Hyung Park, D. H. Cobden, J. M. Atkin, and M. B. Raschke, Nat. Commun. **6**, 6849 (2015).

[40] V. S. Vikhnin, S. Lysenko, A. Rua, F. Fernandez, and H. Liu, Solid State Commun. **137**, 615 (2006).

[41] M. S. Laad, L. Craco, and E. Müller-Hartmann, Phys. Rev. B **73**, 195120 (2006).

[42] M. Gatti, F. Bruneval, V. Olevano, and L. Reining, Phys. Rev. Lett. **99**, 266402 (2007).

[43] K. Chenoweth, A. C. T. van Duin, and W. A. Goddard, J. Phys. Chem. A **112**, 1040 (2008).

[44] Atomistix ToolKit version 2014.2 (QuantumWise A/S, 2014).

[45] J. M. Longo and P. Kierkegaard, Acta Chem. Scand. **24**, 420 (1970).

[46] M. van Veenendaal, Phys. Rev. B **87**, 235118 (2013).

[47] K. H. Bennemann, J. Phys.: Condens. Matter **23**, 073202 (2011).

[48] J. C. Stover, *Optical Scattering Measurement and Analysis* (McGraw-Hill, 2010).

[49] M. Zerrad, M. Lequime, and C. Amra, Appl. Opt. **53**, A297 (2014).

[50] T. Herffurth, S. Schröder, M. Trost, A. Duparré, and A. Tünnermann, Appl. Opt. **52**, 3279 (2013).

[51] J. E. Harvey, S. Schröder, N. Choi, and A. Duparré, Opt. Eng. **51**, 13402 (2012).

[52] J. Sorrentini, M. Zerrad, and C. Amra, Opt. lett. **34**, 2429 (2009).

[53] C. F. Bohren and D. P. Huffman, *Absorption and scattering of light by small particles* (John Wiley, 1983).

[54] H. W. Verleur, A. S. Barker, and C. N. Berglund, Phys. Rev. **172**, 788 (1968).

[55] S. Lysenko, F. Fernández, A. Rúa, and H. Liu, J. Appl. Phys. **114**, 153514 (2013).

[56] S. Lysenko, F. Fernández, A. Rúa, N. Sepúlveda, and J. Aparicio, Appl. Opt. **54**, 2141 (2015).

[57] See Supplemental Material at [url] for relative change of UDC indicatrix movie of VO_2 film on A-cut Al_2O_3.

[58] Z. Tao, F. Zhou, T.-R. T. Han, D. Torres, T. Wang, N. Sepulveda, K. Chang, M. Young, R. R. Lunt, and C.-Y. Ruan, Sci. Rep. **6** (2016).

[59] R. Yusupov, T. Mertelj, V. V. Kabanov, S. Brazovskii, P. Kusar, J.-h. Chu, I. R. Fisher, and D. Mihailovic, Nat. Phys. **6**, 681 (2010).

[60] T. Huber, S. O. Mariager, A. Ferrer, H. Schäfer, J. A. Johnson, S. Grübel, A. Lübcke, L. Huber, T. Kubacka, C. Dornes, C. Laulhe, S. Ravy, G. Ingold, P. Beaud, J. Demsar, and S. L. Johnson, Phys. Rev. Lett. **113**, 026401 (2014).

[61] A. P. Levanyuk and D. G. Sannikov, Sov. Phys. Usp. **17**, 199 (1974).

[62] S. Wall, D. Wegkamp, L. Foglia, K. Appavoo, J. Nag, R. F. Haglund, J. Stähler, and M. Wolf, Nat. Commun. **3**, 721 (2012).

[63] A. Pashkin, C. Kübler, H. Ehrke, R. Lopez, A. Halabica, R. Haglund Jr, R. Huber, and A. Leitenstorfer, Phys. Rev. B **83**, 195120 (2011).

[64] B. A. Strukov and A. P. Levanyuk, *Ferroelectric Phenomena in Crystals: Physical Foundations* (Springer-Verlag, Berlin Heidelberg, 1998).

[65] C. Ott, M. F. Jager, C. J. Kaplan, R. E. Marvel, R. F. Haglund, D. M. Neumark, and S. R. Leone, International Conference on Ultrafast Phenomena, UTu4A 48 (2016).

[66] D. Wegkamp, M. Herzog, L. Xian, M. Gatti, P. Cudazzo, C. L. McGahan, R. E. Marvel, R. F. Haglund, A. Rubio, M. Wolf, and J. Stähler, Phys. Rev. Lett. **113**, 216401 (2014).

[67] Z. Tao, T.-R. T. Han, S. D. Mahanti, P. M. Duxbury, F. Yuan, C.-Y. Ruan, K. Wang, and J. Wu, Phys. Rev. Lett. **109**, 166406 (2012).

[68] M. Liu, M. Wagner, E. Abreu, S. Kittiwatanakul, A. McLeod, Z. Fei, M. Goldflam, S. Dai, M. Fogler, J. Lu, *et al.*, Phys. Rev. Lett. **111**, 096602 (2013).

[69] J. Laverock, S. Kittiwatanakul, A. Zakharov, Y. Niu, B. Chen, S. Wolf, J. Lu, and K. Smith, Phys. Rev. Lett.

113, 216402 (2014).

[70] B. Hong, K. Hu, Z. Tao, J. Zhao, N. Pan, X. Wang, M. Lu, Y. Yang, Z. Luo, and C. Gao, Phys. Rev. B **95**, 075433 (2017).

[71] W.-P. Hsieh, M. Trigo, D. A. Reis, G. Andrea Artioli, L. Malavasi, and W. L. Mao, Appl. Phys. Lett. **104**, 021917 (2014).

[72] L. Bai, Q. Li, S. A. Corr, Y. Meng, C. Park, S. V. Sinogeikin, C. Ko, J. Wu, and G. Shen, Phys. Rev. B **91**, 104110 (2015).

[73] H. He, H. Gao, W. Wu, S. Cao, J. Hong, D. Yu, G. Deng, Y. Gao, P. Zhang, H. Luo, *et al.*, Phys. Rev. B **94**, 205127 (2016).

[74] E. Arcangeletti, L. Baldassarre, D. Di Castro, S. Lupi, L. Malavasi, C. Marini, A. Perucchi, and P. Postorino, Phys. Rev. Lett. **98**, 196406 (2007).

[75] J. Wu, Q. Gu, B. S. Guiton, N. P. de Leon, L. Ouyang, and H. Park, Nano Lett. **6**, 2313 (2006).

[76] J. Cao, E. Ertekin, V. Srinivasan, W. Fan, S. Huang, H. Zheng, J. Yim, D. Khanal, D. Ogletree, J. Grossman, *et al.*, Nature Nanotech. **4**, 732 (2009).

[77] B. Hu, Y. Ding, W. Chen, D. Kulkarni, Y. Shen, V. V. Tsukruk, and Z. L. Wang, Adv. Mater. **22**, 5134 (2010).

[78] A. Tselev, I. Lukyanchuk, I. Ivanov, J. Budai, J. Tischler, E. Strelcov, A. Kolmakov, and S. Kalinin, Nano Lett. **10**, 4409 (2010).

[79] B. Hu, Y. Zhang, W. Chen, C. Xu, and Z. L. Wang, Adv. Mater. **23**, 3536 (2011).

[80] J. Laverock, A. Preston, D. Newby Jr, K. Smith, S. Sallis, L. Piper, S. Kittiwatanakul, J. Lu, S. Wolf, M. Leandersson, *et al.*, Phys. Rev. B **86**, 195124 (2012).

[81] N. B. Aetukuri, A. X. Gray, M. Drouard, M. Cossale, L. Gao, A. H. Reid, R. Kukreja, H. Ohldag, C. A. Jenkins, E. Arenholz, *et al.*, Nat. Phys. **9**, 661 (2013).

[82] S. Kumar, J. P. Strachan, M. D. Pickett, A. Bratkovsky, Y. Nishi, and R. S. Williams, Adv. Mater. **26**, 7505 (2014).

[83] L. Fan, S. Chen, Z. Luo, Q. Liu, Y. Wu, L. Song, D. Ji, P. Wang, W. Chu, C. Gao, *et al.*, Nano Lett. **14**, 4036 (2014).

[84] S. Kittiwatanakul, S. A. Wolf, and J. Lu, Appl. Phys. Lett. **105**, 073112 (2014).